Journal of
Applied
Crystallography
ISSN 0021-8898

Received 10 June 2003
Accepted 14 October 2003

Analysis of the mutual coherence function of X-rays using dynamical diffraction

Hiroshi Yamazaki[a]* and Tetsuya Ishikawa[a,b]

[a]SPring-8/JASRI, Mikazuki, Hyogo 679-5198, Japan, and [b]SPring-8/RIKEN, Mikazuki, Hyogo 679-5148, Japan. Correspondence e-mail: yamazaki@spring8.or.jp

X-ray rocking-curve profiles for a perfect crystal are calculated using the mutual coherence function of the incident wave. The derived result is that the rocking curve to be measured should be a convolution of the intrinsic profile of the crystal reflection with the Fourier transform of the complex degree of coherence of the incident wave. This allows experimental evaluation of the complex degree of coherence from measured rocking-curve profiles with the help of the calculated intrinsic profile. The mutual coherence function of synchrotron X-rays prepared with a conventional Si double-crystal monochromator was mapped as a function of both spatial separation and time delay.

1. Introduction

Coherence in the hard X-ray region is becoming increasingly important with the recent development of third-generation synchrotron light sources. The improved coherence has allowed the introduction of new techniques that take advantage of phase relations. Typical examples include shearing interferometry (Kohmura *et al.*, 2003), phase tomography (Cloetens *et al.*, 1999) and non-crystalline diffraction microscopy (Miao *et al.*, 2003). However, at the third-generation sources, it is spatial or transverse coherence that benefits most, since this is enhanced by a smaller source size and a longer source–observer distance. The temporal or longitudinal coherence, basically determined by the bandwidth of the monochromator, remains unchanged if we use a common Si 111 monochromator. Up to now, the spatial and temporal components of the coherence have usually been treated separately. The spatial coherence is assumed to be preserved by the crystal monochromator, as this does not change the angular divergence if the Bragg reflection is symmetric. The temporal coherence, on the other hand, is enlarged as the bandpass of the monochromator is reduced. Spatial coherence lengths estimated by the van Cittert–Zernike theorem in the above-described treatment are almost always longer than those determined from measurements (Salditt *et al.*, 1994; Baron *et al.*, 1996; Fezzaa *et al.*, 1997; Kohn *et al.*, 2000, 2001; Leitenberger *et al.*, 2001; Yabashi, Tamasaku & Ishikawa, 2001).

More rigorously, the first-order coherence of a light beam is characterized by a mutual coherence function (Born & Wolf, 1999) that is defined as a cross-correlation function of the wavefields at two points with a time delay. Since diffraction by crystals mixes the temporal and spatial coherence when the incident wave has a moderate degree of coherence (Yamazaki & Ishikawa, 2002), separate consideration of spatial and temporal coherence cannot be justified for most X-ray beamlines of synchrotron radiation facilities with various optical components. Therefore, the detailed design of advanced applications of X-ray coherence requires a reliable means of characterization of the mutual coherence function of the beam produced by the optical components.

A rocking-curve profile for a perfect crystal is related to both the angular and the energy spreads of the incident beam (Compton & Allison, 1935). Conventionally, rocking-curve profiles are given as convolutions of profile functions of the incident beam with intrinsic profiles of the crystal reflection, which assume an incident plane wave. The crystal reflection profile functions are sometimes referred to as resolution functions (Cooper & Nathans, 1967). In the profile functions of the incident beam, energy spreads are converted to effective angular spreads as predicted by Bragg's law. Furthermore, according to classical optics, the mutual coherence function is also related to both the angular and the energy spreads of the beam. Accordingly, there should be some connection between the measured rocking-curve profile for a perfect crystal and the mutual coherence function of the incident beam.

In this paper, we have calculated the rocking-curve profile taking into account the mutual coherence function of the incident X-ray wave. The result is that the rocking-curve profile of a perfect crystal is given as a convolution of the intrinsic profile of the crystal reflection with the Fourier transform of the mutual coherence function of the incident wave. Accordingly, we can extract some aspects of the mutual coherence function from the measured rocking-curve profile by solving an inverse problem with the help of a calculated intrinsic profile. The space and time dependence of the mutual coherence function of a monochromatic X-ray beam prepared with a conventional Si double-crystal monochromator in an X-ray undulator beamline has been analysed from the measured rocking-curve profiles of a perfect Si crystal using several collinear reciprocal-lattice vectors.

2. Calculation of a rocking-curve profile

We consider X-ray diffraction in Bragg geometry with a perfect crystal in a single scattering plane including a reciprocal-lattice vector **h**. We will use two distinct oblique coordinate systems, $s_o z_o$ for incident and $s_h z_h$ for reflected waves (Fig. 1), in which the s_o and s_h axes, which intersect at a point O_c on the crystal surface, are respectively parallel to the incident and reflected wavevectors, satisfying the exact Bragg condition in a kinematic sense. At a distance l_o from O_c back along the s_o axis, a point O_o is located where the s_o axis intersects with the z_o axis, which is antiparallel to **h**. Similarly, at a distance l_h from O_c along the s_h axis, a point O_h is located where the s_h axis intersects with the z_h axis, which is also antiparallel to **h**. Suppose that the diffraction modifies an incident quasi-monochromatic X-ray wave $V_o(P, t)$ into an emerging quasi-monochromatic wave $V_h(Q, t)$, where P and Q are points on the z_o and z_h axes, respectively. We denote the position vectors of P and Q as $\mathbf{r}_P$ and $\mathbf{r}_Q$, and the z_o and z_h components of P and Q as z_P and z_Q, respectively. Each wave may be represented as a product of a complex envelope function and a periodic factor related to the central wavenumber K by

$$V_o(P, t) = A_o(P, t)\exp[i(\mathbf{K}_o \cdot \mathbf{r}_P - Kc\,t)] \quad (1)$$

and

$$V_h(Q, t) = A_h(Q, t)\exp[i(\mathbf{K}_h \cdot \mathbf{r}_Q - Kc\,t)], \quad (2)$$

where $\mathbf{K}_o$ and $\mathbf{K}_h$, the central wavevectors, are related to the deviation $\theta_o - \theta_B$ of the incident wave from the Bragg condition:

$$\mathbf{K}_o = K\hat{\mathbf{s}}_o + K(\theta_o - \theta_B)\hat{\mathbf{x}}_o, \;\; \mathbf{K}_h = K\hat{\mathbf{s}}_h + K|b|(\theta_o - \theta_B)\hat{\mathbf{x}}_h. \quad (3)$$

The unit vectors $\hat{\mathbf{s}}_o$ and $\hat{\mathbf{s}}_h$ are along the s_o and s_h axes, respectively, and $\hat{\mathbf{x}}_o$ and $\hat{\mathbf{x}}_h$ are shown in Fig. 1. Then, the following relation holds between the two envelope functions (Yamazaki & Ishikawa, 2002):

$$A_h(Q, t) = (iKC\chi_h/4\sin\theta_B)\int_{-\infty}^{+\infty} \mathrm{d}z_P\, A_o[P, t-(l_o+l_h)/c] \times \exp[i\alpha W(z_P + |b|z_Q)]\,\omega[\alpha(z_P + |b|z_Q)]. \quad (4)$$

A dimensionless complex parameter W representing the deviation from the exact Bragg condition is given by

$$W = \frac{|b|^{1/2}}{2|C|(\chi_h\chi_{\bar{h}})^{1/2}}[2(\theta_o - \theta_B)\sin(2\theta_B) + \chi_o(1 + 1/|b|)], \quad (5)$$

where b is an asymmetry factor and χ_g is the gth Fourier component of the polarizability. A complex parameter α is given by $K|C|(\chi_h\chi_{\bar{h}})^{1/2}/(2|b|^{1/2}\sin\theta_B)$. A propagator function $\omega(\alpha z)$ is then represented using the zeroth- and second-order Bessel functions as

$$\omega(\alpha z) = \begin{cases} J_0(\alpha z) + J_2(\alpha z) & (z > 0), \\ 0 & (z \le 0). \end{cases} \quad (6)$$

The reflected intensity as a function of W is written as

$$\begin{aligned} I_h(W) &= \left\langle \int_{-\infty}^{+\infty} \mathrm{d}z_Q\, |A_h(Q, t)|^2 \right\rangle \\ &= |b||\chi_h/\chi_{\bar{h}}|(\alpha\alpha^*/4) \\ &\quad \times \int_{-\infty}^{+\infty} \mathrm{d}z_Q \int_{-\infty}^{+\infty} \mathrm{d}z_P \int_{-\infty}^{+\infty} \mathrm{d}z'_P\, \Gamma_o(z_P, z'_P) \\ &\quad \times \exp[i\alpha W(z_P + |b|z_Q) - i\alpha^* W^*(z'_P + |b|z_Q)] \\ &\quad \times \omega[\alpha(z_P + |b|z_Q)]\,\omega^*[\alpha(z'_P + |b|z_Q)], \end{aligned} \quad (7)$$

where the angle brackets denote the time average and z'_P is the z_o coordinate of the point P' on the z_o axis. A correlation function appearing in equation (7), $\Gamma_o(z_P, z'_P) = \langle A_o(P, t)A_o^*(P', t)\rangle$, is related to the mutual coherence function $\langle V_o(P, t)V_o^*(P', t)\rangle$ introduced by Wolf (Born & Wolf, 1999) as

$$\langle V_o(P, t)V_o^*(P', t)\rangle = \Gamma_o(z_P, z'_P)\exp[iK(z_P - z'_P)\sin\theta_B]. \quad (8)$$

We define the Fourier transform of $\omega(\alpha z)$ and its inversion as

$$\tilde{\omega}(W) = (i\alpha/2)\int_{-\infty}^{+\infty} \mathrm{d}z\, \omega(\alpha z)\exp(i\alpha Wz), \quad (9)$$

and

$$\omega(\alpha z) = (1/\pi i)\int \mathrm{d}W\, \tilde{\omega}(W)\exp(-i\alpha Wz). \quad (10)$$

Integration over W is performed by changing the variable into θ_o, which has a range from minus infinity to infinity, by the use of equation (5). The analytical expression of the Fourier transform is given by

$$\tilde{\omega}(W) = \begin{cases} -W - (W^2 - 1)^{1/2} & (|W| > 1,\ \mathrm{Re}\{W\} < 0), \\ -W + i(1 - W^2)^{1/2} & (|W| \le 1), \\ -W + (W^2 - 1)^{1/2} & (|W| > 1,\ \mathrm{Re}\{W\} > 0). \end{cases} \quad (11)$$

Using equation (10), equation (7) becomes

$$I_h(W) = (\alpha/2\pi)\int \mathrm{d}W'\, R_i(W')\int_{-\infty}^{+\infty} \mathrm{d}z_P \int_{-\infty}^{+\infty} \mathrm{d}z'_P \times \Gamma_o(z_P, z'_P)\exp[i\alpha(W - W')(z_P - z'_P)], \quad (12)$$

where

$$R_i(W) = |\chi_h/\chi_{\bar{h}}|\,|\tilde{\omega}(W)|^2. \quad (13)$$

The correlation function of an incident beam with a moderate degree of coherence may be represented as

$$\Gamma_o(z_P, z'_P) \simeq I_o(\bar{z}_o)\,g_o(\Delta z_o), \quad (14)$$

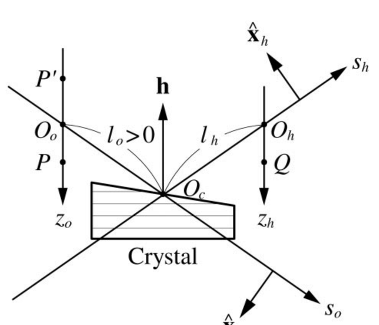

Figure 1
Geometry and coordinate system for representation of Bragg reflection.

using the average location of two points, $\bar{z}_o = (z_P + z'_P)/2$, and their separation, $\Delta z_o = z_P - z'_P$. This is justified when the normalized correlation function $g_o(\Delta z_o)$, or the complex degree of coherence (Born & Wolf, 1999), varies much more rapidly with Δz_o than the intensity distribution $I_o(\bar{z}_o)$ varies with $\bar{z}_o$. Then, the measured rocking-curve profile, or the reflected intensity profile normalized by the incident intensity $\int_{-\infty}^{+\infty} \mathrm{d}\bar{z}_o\, I_o(\bar{z}_o)$, becomes

$$R(W) = \int \mathrm{d}W'\, R_i(W')\, \tilde{g}_o(W - W'), \tag{15}$$

using the Fourier transform of the complex degree of coherence:

$$\tilde{g}_o(W - W') = (\alpha/2\pi) \int_{-\infty}^{+\infty} \mathrm{d}\Delta z_o\, g_o(\Delta z_o) \exp[i\alpha(W - W')\Delta z_o]. \tag{16}$$

The intrinsic profile for the crystal is given by $R_i(W)$, since a monochromatic plane incident wave is characterized as $g_o(\Delta z_o) = 1$. Therefore, $\tilde{g}_o(W - W')$ is equivalent to the profile function of the incident beam in the conventional treatment for the rocking-curve profile (Compton & Allison, 1935).

Application of the convolution theorem for Fourier transforms to equation (15) gives

$$\int \mathrm{d}W\, R(W) \exp(-i\alpha W \Delta z_o) = g_o(\Delta z_o) \int \mathrm{d}W\, R_i(W) \exp(-i\alpha W \Delta z_o), \tag{17}$$

which is reduced to the following equation that connects the complex degree of coherence of the incident beam to the measured and intrinsic rocking-curve profiles:

$$g_o(\Delta z_o) = \frac{\int_{-\infty}^{+\infty} \mathrm{d}\theta_o\, R(\theta_o - \theta_B) \exp[-iK(\theta_o - \theta_B)\Delta z_o \cos\theta_B]}{\int_{-\infty}^{+\infty} \mathrm{d}\theta_o\, R_i(\theta_o - \theta_B) \exp[-iK(\theta_o - \theta_B)\Delta z_o \cos\theta_B]}. \tag{18}$$

The above complex degree of coherence is taken at two different points on a line parallel to a certain reciprocal-lattice vector at the same time. Measured rocking-curve profiles for various reflections give $g_o(\Delta z_o)$ values corresponding to the respective Bragg angles, and consequently we can obtain the two-dimensional distribution of the complex degree of coherence as a function of spatial separation in the scattering plane.

When the angular spread of the incident wave is sufficiently small, we can assume that the complex envelope function $A_o(P, t)$ may propagate along $\mathbf{K}_o$ with little change in form over time. This approximation enables us to convert the complex degree of coherence at the same time into the complex degree of coherence at arbitrary time differences for a given spatial separation along an isochronous wavefront perpendicular to $\mathbf{K}_o$. This is because a spatial separation Δz_o appearing in equation (18) is divided into an effective spatial separation, $\Delta x = \Delta z_o \cos\theta_B$, and an effective temporal separation, $c\Delta t = -\Delta z_o \sin\theta_B$, by projecting it onto the $\hat{\mathbf{x}}_o$ and $-\hat{\mathbf{s}}_o$ directions, since the direction of the spatial separation is inclined from the isochronous wavefront by the Bragg angle. The angular spread φ of the incident wave for which this treatment is valid is estimated roughly as follows. The wavefield starting from P at a time t increases in width by about $c|\Delta t|\varphi$ after a time interval Δt. The quasi-invariance of the complex envelope function is justified when the length is much shorter than a spatial coherence length λ/φ, λ being the average wavelength of the incident beam. The complex degree of coherence taken at two separate times t and $t + \Delta t$ has high values only when $c|\Delta t|$ is shorter than a temporal coherence length $\lambda^2/\Delta\lambda$, $\Delta\lambda$ being the bandwidth. Therefore, the above assumption is valid for the incident beam if $\lambda^2/\Delta\lambda \ll \lambda/\varphi^2$, or $\varphi \ll (\Delta\lambda/\lambda)^{1/2}$. For X-rays prepared with various optical components, including an Si 111 monochromator ($\Delta\lambda/\lambda \simeq 10^{-4}$), the condition $\varphi \ll (\Delta\lambda/\lambda)^{1/2} \simeq 10^{-2}$ rad is certainly satisfied.

3. Experimental and results

The crystal arrangement shown schematically in Fig. 2 was set up at a long undulator beamline at SPring-8, BL19LXU (Yabashi, Mochizuki *et al.*, 2001). The first harmonic from a planar undulator through a front-end slit was further monochromated at a wavelength of 0.661 Å with a double-crystal monochromator (DCM) (Yabashi *et al.*, 1999). The monochromatic X-rays impinged on an analyser crystal that measured the rocking-curve profiles. A calibrated ionization chamber and an Si-PIN detector were placed before and after the analyser crystal, respectively. The crystals in the DCM and the analyser were (111) Si plates. The crystals were aligned to the ($+n$, $-n$, $\pm m$) setting, with 111 and 333 reflections for n, and 111, 333, 444, 555, 777, 888 and 999 reflections for m. The analyser crystal was mounted on a high-precision goniometer for the rocking-curve measurements (Ishikawa *et al.*, 1992), with a coarse rotation stage attached to make the reflection indices easy to change. A series of rocking-curve profiles were measured by stepping the analyser crystal. From each profile, we calculated $g_o(\Delta z_o)$ of equation (18) using the atomic scattering factors reported by Sasaki (1984).

Fig. 3 shows some of the absolute values of the simultaneous complex degrees of coherence analysed for n = 111 as functions of the spatial separation Δz_o. The spatial separations were inclined from the isochronous wavefront by 6.05, −6.05 and 71.64° for the 111, $\bar{1}\bar{1}\bar{1}$ and 999 reflections of the analyser crystal, respectively. The peak values of the analysed functions were close to unity. The small differences from unity were caused both by the errors of the base lines of the detectors and by the finite angular ranges of the rocking-curve measure-

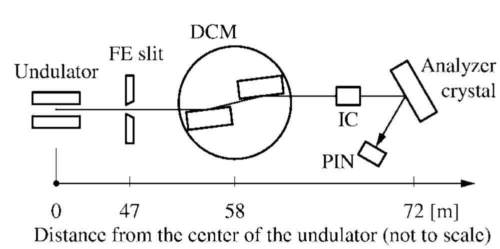

Figure 2
Experimental setup (front view). The aperture of the front-end (FE) slit was set at 1 × 1 mm. DCM: double-crystal monochromator; IC: ionization chamber; PIN: Si-PIN detector.

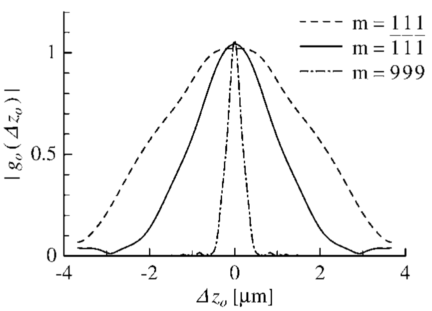

Figure 3
The simultaneous complex degrees of coherence analysed for n = 111.

ments. The width of the complex degree of coherence analysed for m = 111 agreed with the experimental result found by using a wavefront-dividing interferometer (Yamazaki & Ishikawa, 2003).

Fig. 4 shows the space–time distributions for the absolute values of the complex degrees of coherence for $\Delta t \neq 0$, analysed for (*a*) n = 111 and (*b*) n = 333. The vertical and horizontal axes indicate the effective spatial separation Δx and the effective temporal separation $c\Delta t$, respectively. The contours show the positions where the absolute values of the functions are 0.8, 0.6, 0.4 and 0.2, going from the inside outwards. The areas with a high degree of coherence were inclined toward the directions of the reciprocal-lattice vectors of the crystals in the DCM. These results confirm the theoretical consideration that coherence is modified in the direction of the reciprocal-lattice vector of a crystal (Yamazaki & Ishikawa, 2002). The temporal coherence length of the X-rays monochromated with the 333 crystals was longer than that with the 111 crystals.

4. Summary and conclusions

We have calculated the X-ray rocking-curve profiles for a perfect crystal taking into account the mutual coherence function of the incident wave. The rocking-curve profile to be measured is represented as the convolution of the intrinsic profile of the crystal reflection with the Fourier transform of the complex degree of coherence of the incident wave. This allows experimental evaluation of the complex degree of coherence from measured rocking-curve profiles with the help of the calculated intrinsic profile. We mapped the complex degree of coherence of synchrotron X-rays produced with an Si double-crystal monochromator as a function of both the effective spatial separation and the temporal separation.

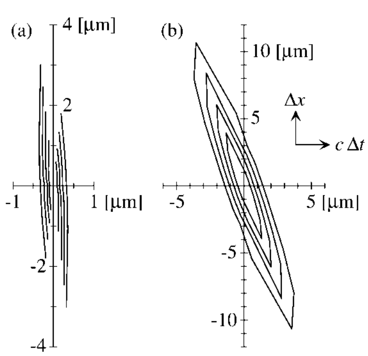

Figure 4
The space–time distributions for the complex degrees of coherence for Δt $\neq$ 0 analysed for (*a*) n = 111 and (*b*) n = 333.

The analysed space–time distributions do not allow the separate consideration of the spatial and temporal coherence for the monochromated X-ray beams. Generally, the coherence of an X-ray beam produced by optical components has to be characterized by its space–time distribution. Quantification of the mutual coherence will facilitate design of advanced applications, especially in using X-rays with full spatial coherence emitted from forthcoming X-ray free-electron lasers (Arthur, 2002; Wagner, 1999; Shintake *et al.*, 2001).

We are grateful to Dr J. Sutter for his critical reading of the manuscript.

References

Arthur, J. (2002). *Rev. Sci. Instrum.* **73**, 1393–1395.
Baron, A. Q. R., Chumakov, A. I., Grünsteudel, H. F., Grünsteudel, H., Niesen, L. & Rüffer, R. (1996). *Phys. Rev. Lett.* **77**, 4808–4811.
Born, M. & Wolf, E. (1999). *Principles of Optics*, 7th ed. Cambridge University Press.
Cloetens, P., Ludwig, W., Baruchel, J., Dyck, D. V., Landuyt, J. V., Guigay, J. P. & Schlenker, M. (1999). *Appl. Phys. Lett.* **75**, 2912–2914.
Compton, A. H. & Allison, S. K. (1935). *X-rays in Theory and Experiment*, 2nd ed. New York: Van Nostrand.
Cooper, M. J. & Nathans, R. (1967). *Acta Cryst.* **23**, 357–367.
Fezzaa, K., Comin, F., Marchesini, S., Cösson, R. & Belakhovsky, M. (1997). *J. X-ray Sci. Technol.* **7**, 12–23.
Ishikawa, T., Yoda, Y., Izumi, K., Suzuki, C. K., Zhang, X. W., Ando, M. & Kikuta, S. (1992). *Rev. Sci. Instrum.* **63**, 1015–1018.
Kohmura, Y., Ishikawa, T., Takano, H. & Suzuki, Y. (2003). *J. Appl. Phys.* **93**, 2283–2285.
Kohn, V., Snigireva, I. & Snigirev, A. (2000). *Phys. Rev. Lett.* **85**, 2745–2748.
Kohn, V., Snigireva, I. & Snigirev, A. (2001). *Opt. Commun.* **198**, 293–309.
Leitenberger, W., Kuznetsov, S. M. & Snigirev, A. (2001). *Opt. Commun.* **191**, 91–96.
Miao, J., Hodgson, K. O., Ishikawa, T., Larabell, C. A., LeGros, M. A. & Nishino, Y. (2003). *Proc. Natl Acad. Sci. USA*, **100**, 110–112.
Salditt, T., Rhan, H., Metzger, T. H., Peisl, J., Schuster, R. & Kotthaus, J. P. (1994). *Z. Phys. B*, **96**, 227–230.
Sasaki, S. (1984). *Anomalous Scattering Factors for Synchrotron Radiation Users, Calculated Using Cromer and Liberman's Method*, KEK Report 83–22, National Laboratory for High Energy Physics, Japan.
Shintake, T., Matsumoto, H., Ishikawa, T. & Kitamura, H. (2001). *Proc. SPIE*, **4500**, 12–23.
Yabashi, M., Mochizuki, T., Yamazaki, H., Goto, S., Ohashi, H., Takeshita, K., Ohata, T., Matsushita, T., Tamasaku, K., Tanaka, Y. & Ishikawa, T. (2001). *Nucl. Instrum. Methods A*, **467–468**, 678–681.
Yabashi, M., Tamasaku, K. & Ishikawa, T. (2001). *Phys. Rev. Lett.* **87**, 140801.
Yabashi, M., Yamazaki, H., Tamasaku, K., Goto, S., Takeshita, K., Mochizuki, T., Yoneda, Y., Furukawa, Y. & Ishikawa, T. (1999). *Proc. SPIE*, **3773**, 2–13.
Yamazaki, H. & Ishikawa, T. (2002). *J. Appl. Cryst.* **35**, 314–318.
Yamazaki, H. & Ishikawa, T. (2003). *J. Appl. Cryst.* **36**, 213–219.
Wagner, A. (1999). *Nucl. Phys. B* (*Proc. Suppl.*) **79**, 643–651.